Journal of Materials Chemistry A

ROYAL SOCIETY OF CHEMISTRY

PAPER

View Article Online
View Journal | View Issue

Cite this: J. Mater. Chem. A, 2023, 11, 4162

Carbon quantum dots aqueous solution as electrolyte for H_2O_2 production based on photoelectrochemical water splitting†

Na Wang, Yong-Shuai Zhang, Dong-Dong Wei, Hui-Min Duan, Liu-Meng Mo and Hong-Yan Wang *

Modulation of electrolyte to tailor the activity and selectivity for photoelectrochemical (PEC) water splitting has been long neglected. Herein, we boosted H_2O_2 accumulation on a $BiVO_4$ photoanode *via* PEC water oxidation in a series of carbon quantum dots (CQDs) aqueous solutions with aliphatic amino acids as precursors. Mott–Schottky measurements demonstrated CQDs solution can tune catalytic voltage location of the $BiVO_4$ substrate. Open circuit voltage decay (OCVD) demonstrated that the system can achieve efficient charge separation owing to the fabricated dynamic heterojunction between CQDs particles and $BiVO_4$ substrate. Owing to the energy gradient, water oxidation may occur on the more hydrophilic CQDs surface, which regulated H_2O_2 generation mediated by the formation of hydroxyl radicals ($OH^{\bullet}$) from water, as evidenced by electron paramagnetic resonance (EPR). Assisted by a Clark electrode and linear sweep voltammetry, we evidenced that CQDs can efficiently retard H_2O_2 decomposition. Overall, H_2O_2 production was performed with a rate averaging 0.33 μmol min^{-1} cm^{-2} at 1.23 V with a Faraday efficiency (FE) of 93.5%, in which O_2 evolution was nearly completely suppressed. By contrast, the commonly used HCO_3^- electrolyte only afforded an H_2O_2 evolution rate of 0.032 μmol min^{-1} cm^{-2}, corresponding to FE of 18.2%. Here, we executed PEC water oxidative H_2O_2 accumulation in CQDs solution directly, and the innovation can hopefully draw more attention to catalytic media for improving PEC performance.

Received 5th December 2022
Accepted 18th January 2023

DOI: 10.1039/d2ta09453c

rsc.li/materials-a

1. Introduction

Hydrogen peroxide (H_2O_2) production on an anode, associated with H_2 generation on a cathode, adds much more value for photoelectrochemical (PEC) water splitting.[1–4] Until now, many efforts have been devoted to water oxidative H_2O_2 production,[5–16] but practical and effective protocols are still difficult to come by. This dominantly roots from the challenging issue of suppressing the competitive O_2 evolution, because the two-electron-mediated H_2O_2 generation (*i.e.*, H_2O_2/H_2O, E° = 1.76 V) is less thermodynamically favorable than the subsequent four-electron O_2 evolution reaction (OER) (*i.e.*, O_2/H_2O, E° = 1.23 V).[3,8,17] Additionally, H_2O_2 disproportionation into O_2 and H_2O can be accelerated on the photoanode, which further increases the decomposition of H_2O_2.[2,12,14,18] Therefore, to increase H_2O_2 accumulation, the desired system should both significantly promote H_2O_2 generation and effectively prevent it from serious decomposition.[7,8] It has been identified that the traditional photoanode fabrication *via* nanostructuring,[13] heteroatom doping,[7,10] as well as heterojunction construction[13] can furnish efficient H_2O_2 production from water, but serious degradation of H_2O_2 on the photoanode still unavoidably occurs. Recently, a SnO_{2-x} overlayer coated $BiVO_4$ photoanode achieved great success in water oxidative H_2O_2 generation, accompanied by the efficient inhibition of H_2O_2 decomposition, which endorses such a strategy.[8]

As compared with photoanode fabrication, selection of an appropriate electrolyte is a much more convenient and effective way to try to improve PEC water splitting.[3,4,19] This is because the electrolyte used in PEC and other electrochemistry (EC) systems plays a vital role in charge migration and mass diffusion, and thus has a remarkable influence on catalytic behavior.[20–22] However, until now, little attention has been paid to tailoring PEC performance through the modulation of electrolyte medium. Recently, we demonstrated that a carbon quantum dots (CQDs) aqueous solution generated from EDTA·2Na can act as an electrolyte for PEC water oxidative O_2 production on α-Fe_2O_3 photoanodes with robust efficiency and durability.[23] It was found that the negatively charged CQDs particles and α-Fe_2O_3 substrate can form a dynamic heterojunction to trigger efficient charge separation during the PEC process. Moreover, the CQDs solution can regulate and stabilize the water splitting

Key Laboratory for Macromolecular Science of Shaanxi Province, School of Chemistry and Chemical Engineering, Shaanxi Normal University, Xi'an, 710119, China. E-mail: hongyan-wang@snnu.edu.cn

† Electronic supplementary information (ESI) available. See DOI: https://doi.org/10.1039/d2ta09453c

product by tuning the catalytic voltage location *via* the interaction between the interface of the reaction medium and catalytic material. Therefore, we proposed that operating PEC water splitting in an appropriate CQDs solution in combination with an appropriate photoanode can direct water oxidation into H_2O_2 production rather than the competitive 4-electron transfer for O_2 evolution. More importantly, the degradation of H_2O_2 on the photoanode can hopefully also be prevented. These features are considered to regulate the PEC water oxidation selectivity and improve H_2O_2 accumulation by guiding the pronounced synergy of electrolyte and photocatalyst. Here, we investigated a series of new CQDs aqueous solutions with linear aliphatic amino acids as precursors, in which PEC water oxidation on a $BiVO_4$ photoanode exhibited far superior ability for H_2O_2 accumulation compared with the commonly used HCO_3^- electrolyte. The related mechanism was also studied in detail.

2. Results and discussion

2.1 Fabrication and characterization of CQDs

The preparation of CQDs was carried out *via* hydrothermal treatment, in which 3-aminopropanoic acid, 4-aminobutanoic acid and 6-aminocaproic acid were selected as precursors. After purification and freeze-drying, three CQDs samples were isolated, designated 3-CQDs, 4-CQDs and 6-CQDs, respectively. High-resolution transmission electron microscopy (HR-TEM) indicates the fabricated CQDs consisted of spherical nanoparticles with uniform diameters of 3–6 nm. Both graphitic and amorphous forms of carbon were detected, typically with lattice fringes in the graphitic regions corresponding to (100) interlayer spacing of 2.1 Å in CQDs (Fig. 1a).[24] In powder X-ray diffraction (XRD) spectra, each sample showed a broad peak centered around 24.9°, 23.7° and 23.4°, respectively, which was related to the respective lattice spacing of 3.5 Å in 3-CQDs, 3.7 Å in 4-CQDs and 3.8 Å in 6-CQDs, consistent with the (200) reflection of disordered graphitic-like material (Fig. 1b).[25–27]

When the CQDs samples were dispersed in water, transparent solutions were obtained, indicating the great hydrophilic nature of CQDs. Typically, the aqueous solution of 6-CQDs displayed a characteristic absorption band ranging from 300 to 400 nm ascribed to $\pi \rightarrow \pi^*$ (C=C) conjugated structure transition, followed by an absorption tail extending to the visible light region (Fig. 1c).[27,28] Impressively, 6-CQDs exhibited the widest absorption band in the visible light region as compared with 3-CQDs and 4-CQDs. The fluorescence emission profile is further displayed in Fig. S1,† which exhibits typical excitation-wavelength-dependent behavior for CQDs.[26,29] Along with the excitation wavelength moving from 350 to 410 nm, the maximum of 3-CQDs shifted from $\lambda = 402$ to 478 nm. With the extension of the carbon chain in the corresponding parent precursor, CQDs displayed gradually stronger luminescence intensity, accompanied by a red-shift of the emission spectra. Typically, under identical excitation conditions, 6-CQDs exhibited the strongest luminescence (Fig. 1d). In combination with UV-vis absorption, this implied that 6-CQDs can hold the greatest charge carrier concentration, which may indicate great influence on visible light-driven reaction activity.[30–32] Additionally, the zeta potential of the samples was examined, showing negative values (Fig. 1e and S2†), which implied the negatively-charged CQDs particles can move directionally to the hole-accumulated photoanode plate under electrostatic force during the PEC process.[23,33]

It was noted that CQDs samples were difficult to keep totally dry, which implied their surfaces were likely capped with abundant hydrophilic groups.[34] In their infrared (IR) spectra, 6-CQDs exhibited two strong features at ~1550 and ~1411 cm^{-1}, corresponding to anti-symmetric and symmetric stretches of C=O groups, with stretching vibrations of O–H at ~3128 and ~2938 cm^{-1} (Fig. S3a†).[26,27] Another clear signal at ~3689 cm^{-1} belonged to the stretching vibrations for the N–H bond in –NH–C or –CONH–.[35] Similar signals were observed in 4-CQDs (Fig. S3b†), although with slight shift. The IR spectrum of 3-CQDs displayed a stretching vibration band for O–H at ~3028 cm^{-1}, accompanied by anti-symmetric and symmetric stretches of C=O centered at ~1590 cm^{-1} (Fig. S3c†).[26] Significantly, the N–H signal in 3-CQDs was much broader than that in 4-CQDs and 6-CQDs, implying NH_2 groups were incorporated. The ^{13}C NMR spectra of CQDs and their corresponding precursors are shown in Fig. 1f. Clearly, the spectra profiles are different in each group, suggesting the successful generation of CQDs. In ^{13}C NMR, 6-CQDs exhibited a variety of carbon environments, including –COOH and –CONHC groups, and 3-CQDs displayed two signals close together in the –COOH range. In the same range, 4-CQDs showed a single signal ascribed to –COOH groups. X-ray photoelectron spectroscopy (XPS) in Fig. 1g depicts the high-resolution C 1s spectra, which are deconvoluted into three signals. The lowest energy contribution peaks centered at 285.8 eV and 288.1 eV represented the presence of C–N and C=O groups, respectively. The signals at 284.7 eV belonged to C=C environment, corresponding to sp^2-hybridized graphitic carbon atoms.[36–38] Clearly, 6-CQDs can incorporate more conjugated C=C groups than 3-CQDs and 4-CQDs. It is accepted that π-conjugated structures can show excellent hole-transporting properties, which implies that 6-CQDs enables the best hole migration to be achieved in the system.[39] In the O 1s spectra, the peaks at 531.0 eV and 531.7 eV belonged to O=C and O–C species, respectively (Fig. 1h).[31,40,41] In the high-resolution N 1s spectra, the peak at 399.3 eV corresponded to pyridine-like nitrogen, indicating the doped N was exposed on the surface of CQDs.[42] The signal situated at binding energy 400.5 eV corresponded to C–NH–C, and that at 401.2 eV demonstrated the presence of C=C–NH_2 (Fig. 1i).[29,40] Typically, a band centered at 402 eV was found in the spectrum of 6-CQDs, which was correlated with the –CONHC group.[43] As a comparison, the proportion of C=C–NH_2 bonding was decreased in the order from 3-CQDs, 4-CQDs to 6-CQDs, and 4-CQDs incorporated a slightly higher proportion of the hydrophobic C–NH–C component. It should be noted that 3-CQDs and 6-CQDs presented a smaller contact angle than 4-CQDs in the water droplets experiments exhibited in Fig. 1j, featuring a better hydrophilic character of the surfaces, which implied that 6-CQDs and 3-CQDs expose more

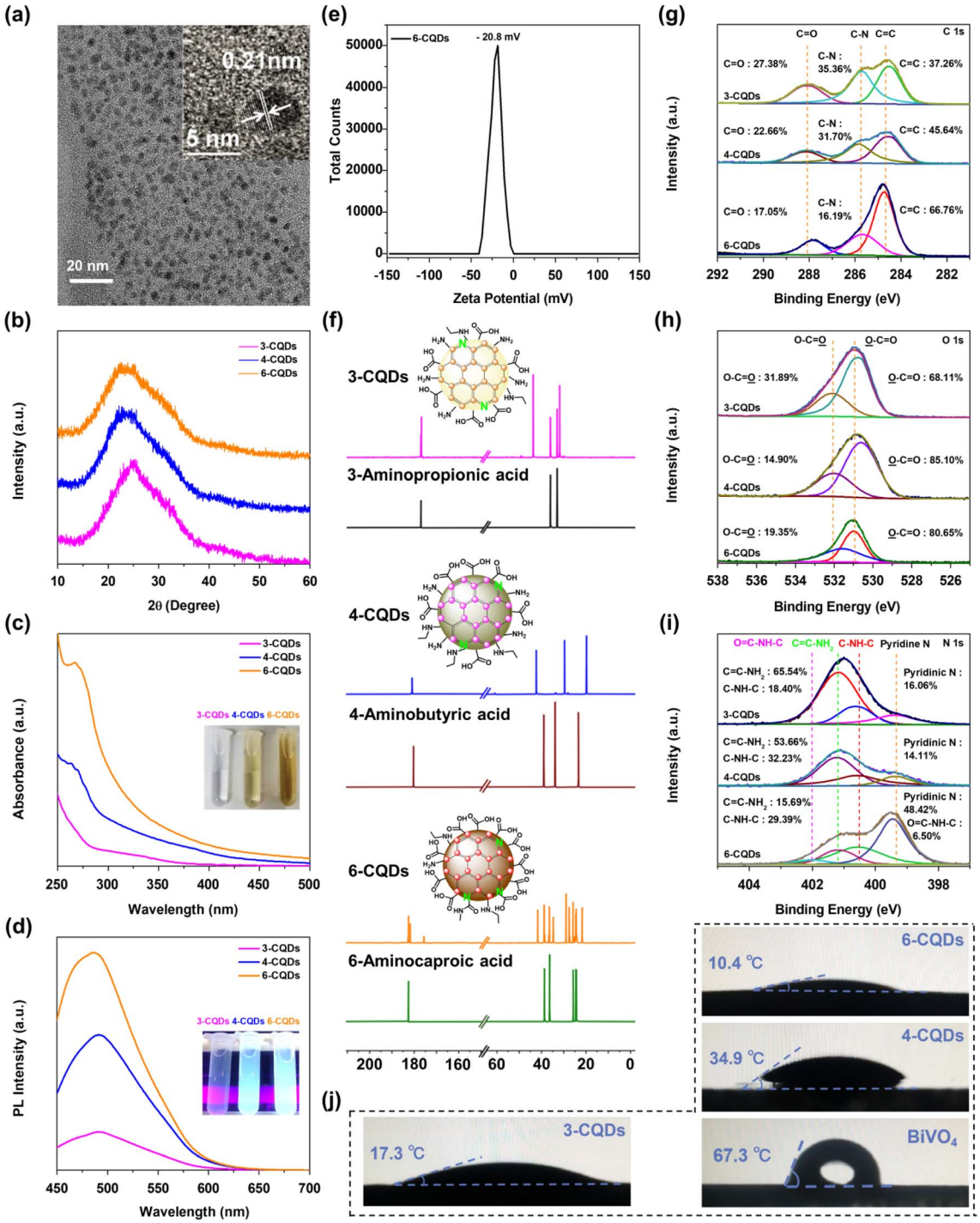

Fig. 1 (a) HR-TEM image of 6-CQDs, and inset showing lattice spacing of 0.21 nm, which corresponds to the (100) plane of graphitic structure; (b) the XRD spectra of CQDs samples; (c) UV-vis spectra and (d) photoluminescence spectra of CQDs samples in water; (e) the zeta potential of 6-CQDs; (f) the ^{13}C NMR spectra of CQDs and their corresponding parent precursors in D_2O, with insets showing the proposed surface components of each CQDs compound; high-resolution C 1s (g), O 1s (h) and N 1s (i) XPS spectra of CQDs samples; (j) contact angles of CQDs samples and $BiVO_4$ substrate in water droplets experiments.

abundant –COOH or –NH_2 groups than 4-CQDs. In line with our combined characterization results, the surface components of each material are proposed in the inset of Fig. 1i. As exhibited in Fig. 1j, all three CQDs samples indicated much better hydrophilic properties than the $BiVO_4$ substrate. It has been perceived that a more hydrophilic surface facilitates confinement of water molecules, and further exerts a serious influence on the generation and conversion of the related intermediates, which thus can tune the PEC activity and even selectivity.[44,45]

2.2 PEC water oxidative activity and selectivity for H_2O_2 production on $BiVO_4$ photoanode in CQDs solution

The performance of PEC H_2O_2 generation on $BiVO_4$ photoanode in CQDs solution was examined with linear sweep voltammetry (LSV) under the irradiation of commercial LEDs ($\lambda = 420$ nm). As expected, the photo-electronic response in each CQDs solution greatly surpassed that in the aqueous solution containing the corresponding parent compounds, and showed a distinct cathodic shift of onset potential (Fig. 2a and S4). Furthermore, $KHCO_3$ aqueous solution with identical electro-conductibility to CQDs was employed for reference. It is generally recognized that concentrated HCO_3^- electrolyte is so far the most efficient catalytic medium for the direct production of H_2O_2 from water oxidation,[8,11–14,16,19] although recent studies have pointed out that the HCO_3^- anion can react with H_2O_2 to prompt its consumption.[2,46,47] Fig. 2a depicts the LSV curves of the $BiVO_4$ photoanode in three CQDs solutions and in $KHCO_3$ aqueous solution. In the darkness, the current ascribed to the EC process for water oxidation was negligible. Under irradiation, 3-CQDs presented 0.91 mA cm^{-2} photocurrent density at 1.23 V (*vs.* reversible hydrogen electrode, RHE), which was slightly decreased to 0.64 mA cm^{-2} when using 4-CQDs instead. 6-CQDs can achieve a more robust activity, with 1.14 mA cm^{-2} at 1.23 V, and the photocurrent displayed a sustained increase over the entire potential range. HCO_3^- electrolyte initiated a photocurrent density of 0.49 mA cm^{-2} at 1.23 V, which was far less than the CQDs solution. We noted that CQDs can sustain a stable photocurrent over long periods of time, suggesting robust stability and durability in the PEC system (Fig. S5†).

Since the competitive 4-electron transfer water oxidative O_2 evolution always occurs, the ability of CQDs solution for H_2O_2 generation on $BiVO_4$ photoanode was examined. As prolonged photo-electrolysis could inevitably lead to the decomposition of H_2O_2, the PEC system was placed in baths of ice (below 5 °C) with continuous illumination for 600 s at 1.23 V. The identification and quantification of H_2O_2 were based on the *N*,*N*-diethyl-1,4-phenylene-diamine (DPD) method (Fig. S6 and S7†).[8] The amounts of O_2 were detected and evaluated by gas chromatography (GC). The results indicated that H_2O_2 generation in 3-CQDs solution was dominant, showing a total amount of 2.18 μmol. 4-CQDs solution was active for both O_2 and H_2O_2 generation, in which the evolution of H_2O_2 was evaluated as 0.51 μmol, accompanied by O_2 production of 0.06 μmol (Fig. 2b). However, since 4-CQDs can react with DPD indicator directly for an unclear reason (Fig. S7b†), the following research was concentrated on 3-CQDs and 6-CQDs. Importantly, 6-CQDs performed better for H_2O_2 production, and the O_2 evolution was nearly completely suppressed. This system produced 3.31 μmol H_2O_2, at a rate of up to 0.33 μmol min^{-1} cm^{-2}. Increasing the bias to 1.5 V, the rate could be improved to 0.42 μmol min^{-1} cm^{-2} (Fig. S8†). Typically, 6-CQDs afforded a Faraday efficiency (FE) of 93.5% for H_2O_2 production at 1.23 V. In sharp contrast, the H_2O_2 evolution rate in HCO_3^- electrolyte was only 0.032 μmol min^{-1} cm^{-2}, corresponding to an FE of 18.2% (Fig. 2b).

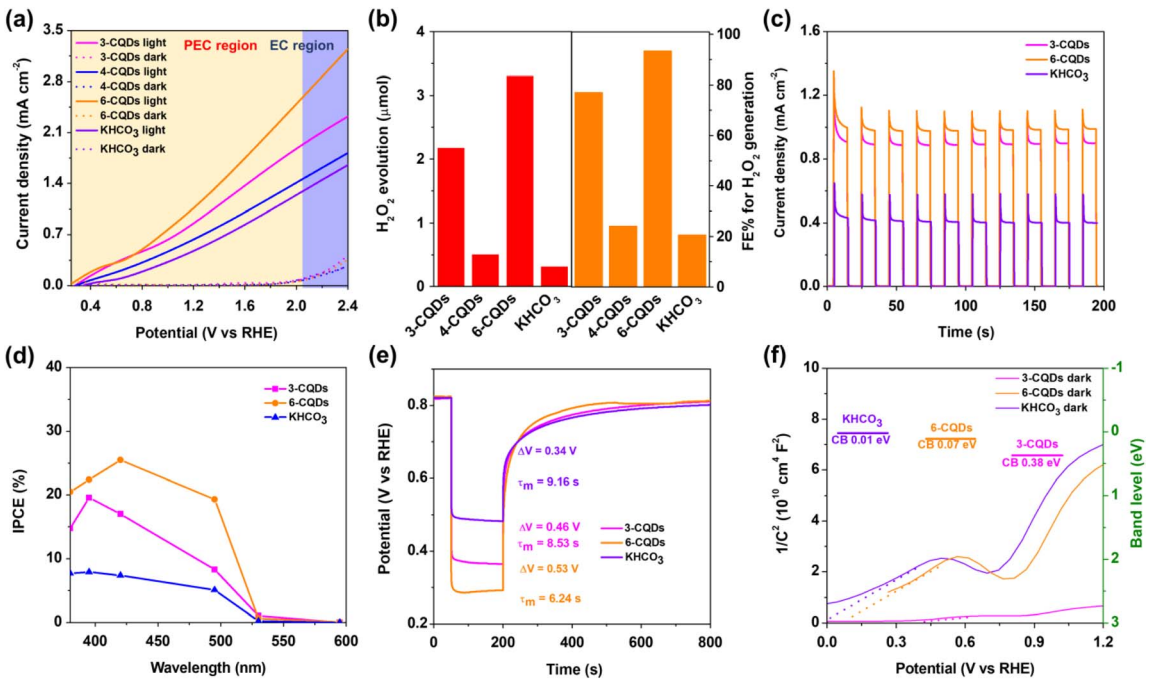

Fig. 2 (a) The LSV of $BiVO_4$ photoanode in CQDs aqueous solution and $KHCO_3$ electrolyte in the dark or under irradiation of 420 nm LED lamp (the input optical power is 8.37 mW cm^{-2}); (b) the yield of H_2O_2 and FE% for H_2O_2 generation; (c) chopped light irradiation curves with 420 nm LED of $BiVO_4$ photoanode in CQDs aqueous solution and $KHCO_3$ electrolyte; (d) IPCE of $BiVO_4$ photoanode in 3-CQDs, 6-CQDs and $KHCO_3$ aqueous solution under different excitation wavelengths; (e) OCVD plots of $BiVO_4$ photoanode in 3-CQDs, 6-CQDs and $KHCO_3$ aqueous solution in the dark or under irradiation of 420 nm LED lamp from the electrolyte–electrode side (ΔV is the difference in voltage between dark and illumination conditions); (f) Mott–Schottky plots of $BiVO_4$ photoanode in 3-CQDs, 6-CQDs and $KHCO_3$ aqueous solution under irradiation.

2.3 Mechanistic study for PEC water oxidative H_2O_2 production in CQDs solution

Fig. 2c illustrates the transient photocurrent responses *versus* time with chopped light irradiation, which brings out the reproducible photocurrent with almost identical value for each on/off cycles, highlighting the satisfied stability for PEC performance. Moreover, the photo-response was very sensitive to the light, regularly increasing or falling off to the baseline as the light was switched on or off, which suggests the facile charge transport.[29,37]

Incident photon-to-current conversion efficiency (IPCE) profiles were recorded with the bias at 1.23 V under continuous illumination. In both CQDs and $KHCO_3$ solutions, the photo-response extended to 530 nm, corresponding to a band gap for $BiVO_4$ of 2.35 eV.[48] Significantly, $BiVO_4$ in 6-CQDs solution yielded a much higher value at each wavelength (Fig. 2d). Based on a broad arsenal of related reports, the improvement in IPCE originates from the efficient separation of photo-generated electron–hole pairs.[48,49] Therefore, the photovoltage–time (V–t) spectrum was recorded based on open circuit voltage decay (OCVD),[50] from which photovoltage (ΔV) was extracted.[51] As shown in Fig. 2e, $BiVO_4$ presented ΔV of 0.34 V in $KHCO_3$ solution, which was increased to 0.46 V in 3-CQDs and 0.53 V in 6-CQDs solutions, respectively. This means that CQDs solutions enable better charge separation.[51] The average charge decay lifetime of the V–t profile provides the carrier lifetime in the structures of semiconductor devices, here demonstrating that the harmonic mean of lifetime τ_m for $BiVO_4$ was 9.16 s in $KHCO_3$, 8.53 s in 3-CQDs and 6.24 s in 6-CQDs, respectively. Clearly, CQDs solution has the better ability to deactivate the surface trap state,[52] suggesting that the photo-generated charge carriers can survive to participate in the water splitting reaction instead being deactivated by surface traps, and thus PEC performance was dramatically enhanced.[51]

Furthermore, the band location of the photoanode in CQDs and $KHCO_3$ was determined based on Mott–Schottky plots (Fig. 2f). Notably, the flat band potential (V_{fb}) of $BiVO_4$ was pinned under dark and illumination conditions.[8] Under irradiation, $BiVO_4$ exhibited positive slopes in Mott–Schottky plots, as for n-type semiconductor.[53,54] The plots indicated that V_{fb} of $BiVO_4$ in HCO_3^- electrolyte was 0.01 V, which was positively shifted to 0.38 V and 0.07 V in 3-CQDs and 6-CQDs solution, respectively. Since an n-type semiconductor has negligible gap between V_{fb} and the bottom edge of the conduction band (CB),[55] it is evident that CQDs solution can cause the CB level of $BiVO_4$ to shift downward.[56–58] As characterized in IPCE, the $BiVO_4$ photoanode showed an energy gap (E_g) of 2.35 eV. Accordingly, the valence band (VB) of $BiVO_4$ in 3-CQDs and 6-CQDs solution was located at 2.73 and 2.42 eV, respectively. Also from CV measurement, the HOMO and LUMO levels for 3-CQDs were evaluated as 2.15 eV and 0.23 eV, respectively (Fig. S9a†).[59] Switching into 6-CQDs, the levels were 1.97 eV and 0.04 eV, respectively (Fig. S9b†). In this sense, the fabricated band edge alignment between $BiVO_4$ and CQDs allows establishment of a type II heterojunction configuration, in which the electrons can migrate from the LUMO band of CQDs to the CB of $BiVO_4$, and holes can move from the VB of $BiVO_4$ to the HOMO of CQDs (Fig. 3a).[59–61] As a result, the charge separation can be efficiently improved.

Further, electron paramagnetic resonance (EPR) measurements were used to monitor the potential radicals for H_2O_2 generation. With the help of 5,5-dimethyl-1-pyrroline-*N*-oxide (DMPO), EPR signals were captured from 6-CQDs solution under identical PEC conditions (Fig. 3b). Simulated by Simfonia software, a sextet featuring an approximate intensity ratio of 1 : 1 : 1 : 1 : 1 : 1 ($\alpha_N = 15.4$ G, $\alpha_H = 22.7$ G) was identified, suggesting the formation of DMPO-C adduct.[62] This agrees with the above proposal that photo-generated holes can migrate to CQDs and then be exhausted, yielding carbon radicals. The proportion of DMPO-C species is 85.3%, and the other 14.7% response comprises a quartet of peaks with an approximate intensity ratio of 1 : 2 : 2 : 1 ($\alpha_N = 14.9$ G, $\alpha_H = 14.7$ G), which corresponds to a DMPO-OH adduct.[8,63] That CQDs can keep integrity after a long period of photoelectrolysis demonstrated the high stability and durability of CQDs during the PEC process (Fig. S5 and S10†). More importantly, combined with the fact that the ˙OH signal was correlated with the formation of H_2O_2,[15,17,64] this implied that in the CQDs system, water oxidation may occur on the CQDs surface and the formed carbon radical can be recovered to CQDs after oxidizing water. A similar EPR response was measured when 3-CQDs were used (Fig. S11†), but the intensity of ˙OH was weaker, with the proportion decreased to 10.4%. For the $KHCO_3$ system, no clear peak was assigned to ˙OH. This trend is in line with the activity for H_2O_2 production, with the order 6-CQDs > 3-CQDs > $KHCO_3$. Since water oxidation occurred on the $BiVO_4$ photoanode in $KHCO_3$ electrolyte, we proposed that, besides much better charge separation, the higher activity for CQDs is due to the much more hydrophilic surface compared with the $BiVO_4$ substrate. This is because more H_2O molecules can be confined, thus water oxidation was facilitated, leading to an improved performance for H_2O_2 generation.[44,45]

Based on these results, we propose a mechanism for PEC water oxidative H_2O_2 production in CQDs solution (Fig. 3c). As a typical n-type semiconductor, photo-generated electrons on $BiVO_4$ are repelled from the surface into the bulk solid and then diffuse to the counter-electrode through the external circuit for hydrogen production. Holes are left and accumulated on the $BiVO_4$ photoanode, leading to a positively-charged surface,[65] which can further attract negatively-charged CQDs particles. The holes migrate along the energy gradient to the CQDs, which are oxidized by the holes and repulsed from the $BiVO_4$ substrate into solution for water oxidation, and finally recover to their original states and stay in the solution. Owing to such a cycle going back and forth, a dynamic balance of CQDs adsorbing onto or desorbing off the $BiVO_4$ surface can be established. In order to confirm the proposal, an *in situ* UV-vis spectroelectrochemical investigation was conducted, as shown in Fig. 3d and S12,† in which the absorption of CQDs solution varied periodically, manifesting the CQDs can dynamically move out of and into the solution.

Moreover, the decomposition of H_2O_2 in the presence of CQDs or $KHCO_3$ was probed with a Clark electrode, which is a generally used method to quantify O_2 evolution of a system in real time.[66,67] This indicated that HCO_3^- unavoidably

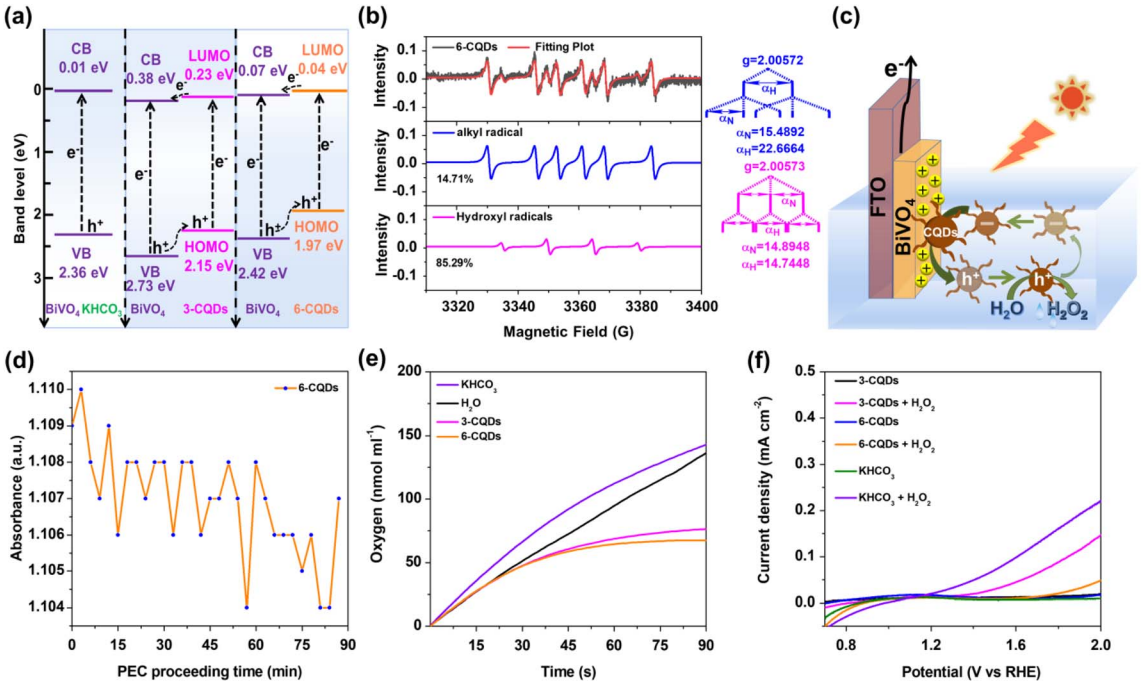

Fig. 3 (a) The determined energy levels of $BiVO_4$ photoanode in $KHCO_3$ electrolyte and CQDs aqueous solutions; (b) experimental EPR spectrum (black) and simulated spectra (blue and pink) of the system after PEC process on $BiVO_4$ photoanode in 6-CQDs solution at 1.23 V for 10 min; (c) the proposed process for water oxidative H_2O_2 production on $BiVO_4$ photoanode in CQDs solution; (d) *in situ* UV-vis absorption at 266 nm for the system with PEC water oxidation on $BiVO_4$ photoanode in 6-CQDs solution; (e) O_2 evolution in a mixture of H_2O_2 and CQDs or $KHCO_3$ aqueous solution (V : V = 1 : 1) determined by Clark electrode under 420 nm irradiation; (f) LSV of $BiVO_4$ photoanode in a mixture of H_2O_2 and CQDs solution (V : V = 7 : 1).

accelerated degradation of H_2O_2 into O_2 either in the dark or under irradiation (Fig. 3e and S13†). This is consistent with previous observations in the literature that one of the difficulties in H_2O_2 accumulation results from the consumption of H_2O_2 by reacting with HCO_3^- anions.[2,46,47] In stark contrast, O_2 evolution in 3-CQDs or 6-CQDs solution was remarkably suppressed under the same conditions, suggesting CQDs can retard the H_2O_2 decomposition. Additionally, Fig. 3f records the LSV curves of $BiVO_4$ with addition of H_2O_2 in different solutions. Compared with HCO_3^- electrolyte, in CQDs solutions the currents that arose from H_2O_2 decomposition were noticeably decreased, further evidencing the sluggish degradation of H_2O_2. Clearly, CQDs can set up a key counterbalance between boosting water oxidation into H_2O_2 generation and retarding H_2O_2 decomposition, which benefits the H_2O_2 accumulation.

3. Conclusions

In summary, we achieved H_2O_2 accumulation on a $BiVO_4$ photoanode *via* PEC water oxidation in a series of CQDs aqueous solutions. Our observations demonstrated that CQDs can feature as both electrolyte and semiconductor, with the following advantages: (1) band edge configuration between CQDs and $BiVO_4$ photoanode allows fabrication of a heterojunction, which enables efficient charge separation; (2) an improved hydrophilic surface provided by CQDs favors confinement of H_2O molecules, which improves PEC water oxidative selectivity to produce H_2O_2; (3) as compared with HCO_3^-, CQDs can prevent H_2O_2 from serious decomposition. As a result, H_2O_2 production in CQDs solution was performed with an average rate of 0.33 μmol min^{-1} cm^{-2} at 1.23 V with a Faraday efficiency of 93.5%, and the competitive O_2 evolution was nearly completely suppressed. Such performance greatly surpassed that which occurred in the commonly used HCO_3^- electrolyte. As a non-parallel example to execute PEC water oxidative H_2O_2 generation in CQDs aqueous solution directly without any other traditional supporting electrolyte, our present work highlights a more striking and facile strategy to tailor the selectivity and activity for PEC water splitting. Subsequently, we have expanded our research to other CQDs systems, aiming for efficient hydrogen production or oxygen reduction based on PEC operation, which work is on-going.

Author contributions

Na Wang: data curation, validation, visualization, formal analysis, writing; Yong-Shuai Zhang: visualization, data curation, formal analysis; Dong-Dong Wei: validation, writing and correcting; Hui-Min Duan: validation, writing and correcting; Liu-Meng Mo: validation, writing and correcting; Hong-Yan Wang: supervision, visualization, formal analysis, conceptualization, writing, editing, reviewing, funding acquisition.

Conflicts of interest

There are no conflicts to declare.

Acknowledgements

We are grateful for the support from National Natural Science Foundation of China (22072082, 21402113), National Natural Science Foundation of Shaanxi Province (2019JQ-175), the Fundamental Research Funds for the Central Universities (GK202103026).

References

1 S. C. Perry, D. Pangotra, L. Vieira, L. L. Csepei, V. Sieber, L. Wang, C. Ponce de León and F. C. Walsh, *Nat. Rev. Chem.*, 2019, **3**, 442–458.
2 C. R. Dong, Y. L. Yang, X. M. Hu, Y. J. Cho, G. Y. Jang, Y. H. Ao, L. Y. Wang, J. Y. Shen, J. H. Park and K. Zhang, *Nat. Commun.*, 2022, **13**, 4982.
3 Y. D. Xue, Y. T. Wang, Z. H. Pan and K. Sayama, *Angew. Chem., Int. Ed.*, 2021, **60**, 10469–10480.
4 J. L. Liu, Y. S. Zou, B. J. Jin, K. Zhang and J. H. Park, *ACS Energy Lett.*, 2019, **4**, 3018–3027.
5 Y. C. Miao and M. F. Shao, *Chin. J. Catal.*, 2022, **43**, 595–610.
6 T. H. Jeon, B. Kim, C. Kim, C. Xia, H. T. Wang, P. J. J. Alvarez and W. Y. Choi, *Energy Environ. Sci.*, 2021, **14**, 3110–3119.
7 T. H. Jeon, H. Kim, H. I. Kim and W. Y. Choi, *Energy Environ. Sci.*, 2020, **13**, 1730–1742.
8 K. Zhang, J. L. Liu, L. Y. Wang, B. J. Jin, X. F. Yang, S. L. Zhang and J. H. Park, *J. Am. Chem. Soc.*, 2020, **142**, 8641–8648.
9 Y. J. Liu, Y. Z. Han, Z. Y. Zhang, W. Zhang, W. Z. Lai, Y. Wang and R. Cao, *Chem. Sci.*, 2019, **10**, 2613–2622.
10 J. H. Baek, T. M. Gill, H. Abroshan, S. Park, X. J. Shi, J. Nørskov, H. S. Jung, S. Siahrostami and X. L. Zheng, *ACS Energy Lett.*, 2019, **4**, 720–728.
11 Y. Miseki and K. Sayama, *Adv. Energy Mater.*, 2019, **9**, 1801294.
12 Y. Miyase, S. Takasugi, S. Iguchi, Y. Miseki, T. Gunji, K. Sasaki, E. Fujita and K. Sayama, *Sustainable Energy Fuels*, 2018, **2**, 1621–1629.
13 X. J. Shi, L. L. Cai, I. Y. Choi, M. Ma, K. Zhang, J. H. Zhao, J. K. Kim, J. K. Kim, X. L. Zheng and J. H. Park, *J. Mater. Chem. A*, 2018, **6**, 19542–19546.
14 K. Fuku, Y. Miyase, Y. Miseki, T. Funaki, T. Gunji and K. Sayama, *Chem.–Asian J.*, 2017, **12**, 1111–1119.
15 X. J. Shi, S. Siahrostami, G. L. Li, Y. R. Zhang, P. Chakthranont, F. Studt, T. F. Jaramillo, X. L. Zheng and J. K. Norskov, *Nat. Commun.*, 2017, **8**, 701.
16 K. Fuku and K. Sayama, *Chem. Commun.*, 2016, **52**, 5406–5409.
17 S. Siahrostami, G. L. Li, V. Viswanathan and J. K. Norskov, *J. Phys. Chem. Lett.*, 2017, **8**, 1157–1160.
18 A. Izgorodin, E. Izgorodina and D. R. MacFarlane, *Energy Environ. Sci.*, 2012, **5**, 9496.
19 D. Pangotra, L. I. Csepei, A. Roth, C. Ponce de León, V. Sieber and L. Vieira, *Appl. Catal., B*, 2022, **303**, 120848.
20 P. T. Xu, T. J. Milstein and T. E. Mallouk, *ACS Appl. Mater. Interfaces*, 2016, **8**, 11539–11547.
21 S. E. Koops, B. C. O'Regan, P. R. F. Barnes and J. R. Durrant, *J. Am. Chem. Soc.*, 2009, **131**, 4808–4818.
22 H. Kusama, H. Orita and H. Sugihara, *Langmuir*, 2008, **24**, 4411–4419.
23 H. Y. Wang, R. Hu, N. Wang, G. L. Hu, K. Wang, W. H. Xie and R. Cao, *Appl. Catal., B*, 2021, **296**, 120378.
24 J. Y. Li, X. R. Yun, Z. L. Hu, L. J. Xi, N. Li, H. Tang, P. C. Lu and Y. R. Zhu, *J. Mater. Chem. A*, 2019, **7**, 26311–26325.
25 Y. M. Hu, Z. L. Zhao, R. Ahmad, M. Harb, L. Cavallo, L. M. Azofra, S. P. Jiang and X. Y. Zhang, *J. Mater. Chem. A*, 2022, **10**, 12713.
26 B. C. M. Martindale, G. A. M. Hutton, C. A. Caputo and E. Reisner, *J. Am. Chem. Soc.*, 2015, **137**, 6018–6025.
27 X. M. Li, S. L. Zhang, S. A. Kulinich, Y. L. Liu and H. B. Zeng, *Sci. Rep.*, 2014, **4**, 4976.
28 S. J. Zhu, Q. N. Meng, L. Wang, J. H. Zhang, Y. B. Song, H. Jin, K. Zhang, H. C. Sun, H. Y. Wang and B. Yang, *Angew. Chem., Int. Ed.*, 2013, **52**, 3953–3957.
29 X. Chen, W. W. Zhang, L. X. Zhang, L. P. Feng, C. X. Zhang, J. Jiang, T. J. Yan and H. Wang, *J. Mater. Chem. A*, 2020, **8**, 18816–18825.
30 J. C. Wang, T. S. Zhou, Y. Zhang, L. Li, C. H. Zhou, J. Bai, J. H. Li, H. Zhu and B. X. Zhou, *ACS Appl. Mater. Interfaces*, 2022, **14**, 45392–45402.
31 B. Q. Wang, Z. R. Deng, X. Z. Fu and Z. H. Li, *J. Mater. Chem. A*, 2018, **6**, 19735–19742.
32 J. Di, J. X. Xia, M. X. Ji, B. Wang, S. Yin, Q. Zhang, Z. G. Chen and H. M. Li, *ACS Appl. Mater. Interfaces*, 2015, **7**, 20111–20123.
33 S. Wang, L. P. Li, Z. H. Zhu, M. L. Zhao, L. M. Zhang, N. N. Zhang, Q. N. Wu, X. Y. Wang and G. S. Li, *Small*, 2019, **15**, 1804515.
34 R. Miao, S. F. Zhang, J. F. Liu and Y. Fang, *Chem. Mater.*, 2017, **29**, 5957–5964.
35 Y. X. Li, Y. Yuan, X. Liang and L. S. Zhao, *ACS Appl. Nano Mater.*, 2022, **5**, 14507–14519.
36 H. J. Yu, Y. F. Zhao, C. Zhou, L. Shang, Y. Peng, Y. H. Cao, L. Z. Wu, C. H. Tung and T. R. Zhang, *J. Mater. Chem. A*, 2014, **2**, 3344.
37 Y. Q. Dong, H. C. Pang, H. B. Yang, C. X. Guo, J. W. Shao, Y. W. Chi, C. M. Li and T. Yu, *Angew. Chem., Int. Ed.*, 2013, **52**, 7800–7804.
38 Z. H. Sheng, L. Shao, J. J. Chen, W. J. Bao, F. B. Wang and X. H. Xia, *ACS Nano*, 2011, **5**, 4350–4358.
39 Z. Iwan, U. M. Javier, G. Paul, A. Juan, G. Giulia, M. O. Agustín, O. Enrique, M. Nazario and K. N. Mohammad, *Adv. Energy Mater.*, 2017, **7**, 1601674.
40 H. J. Jian, R. S. Wu, T. Y. Lin, Y. J. Li, H. J. Lin, S. G. Harroun, J. Y. Lai and C. C. Huang, *ACS Nano*, 2017, **11**, 6703–6716.
41 J. Q. Pan, Y. Z. Sheng, J. X. Zhang, J. M. Wei, P. Huang, X. Zhang and B. X. Feng, *J. Mater. Chem. A*, 2014, **2**, 18082–18086.
42 R. X. Hu, L. L. Li and W. J. Jin, *Carbon*, 2016, **111**, 133–141.
43 R. M. S. Sendão, D. M. A. Crista, A. C. P. Afonso, M. D. V. Martínez de Yuso, M. Algarra, J. C. G. Esteves da Silva and L. P. D. Silva, *Phys. Chem. Chem. Phys.*, 2019, **21**, 20919–20926.

44 Y. Ding, S. Maitra, C. H. Wang, R. T. Zheng, M. Y. Zhang, T. Barakat, S. Roy, J. Liu, Y. Li, T. Hasan and B. L. Su, *J. Energy Chem.*, 2022, **70**, 236–247.
45 Y. L. Yang, S. C. Wang, Y. L. Jiao, Z. L. Wang, M. Xiao, A. J. Du, Y. L. Li, J. S. Wang and L. Z. Wang, *Adv. Funct. Mater.*, 2018, **28**, 1805698.
46 X. J. Yang, Y. H. Duan, J. L. Wang, H. L. Wang, H. L. Liu and D. L. Sedlak, *Environ. Sci. Technol. Lett.*, 2019, **6**, 781–786.
47 D. E. Richardson, H. R. Yao, K. M. Frank and D. A. Bennett, *J. Am. Chem. Soc.*, 2000, **122**, 1729–1739.
48 Y. Pihosh, I. Turkevych, K. Mawatari, T. Asai, T. Hisatomi, J. Uemura, M. Tosa, K. Shimamura, J. Kubota, K. Domen and T. Kitamori, *Small*, 2014, **10**, 3692–3699.
49 S. L. Xie, H. Su, W. J. Wei, M. Y. Li, Y. X. Tong and Z. W. Mao, *J. Mater. Chem. A*, 2014, **2**, 16365–16368.
50 B. Mukherjee, W. Wilson and V. R. Subramanian, *Nanoscale*, 2013, **5**, 269–274.
51 Q. S. Ruan, M. K. Bayazit, V. Kiran, J. J. Xie, Y. Wang and J. W. Tang, *Chem. Commun.*, 2019, **55**, 7191–7194.
52 Y. C. Pu, G. M. Wang, K. D. Chang, Y. H. Ling, Y. K. Lin, B. C. Fitzmorris, C. M. Liu, X. H. Lu, Y. X. Tong, J. Z. Zhang, Y. J. Hsu and Y. Li, *Nano Lett.*, 2013, **13**, 3817–3823.
53 W. Q. Fang, Y. M. Lin, R. Z. Xv and L. Fu, *ACS Appl. Energy Mater.*, 2022, **5**, 11402–11412.
54 M. Y. Huang, J. C. Bian, W. Xiong, C. Huang and R. Q. Zhang, *J. Mater. Chem. A*, 2018, **6**, 3602–3609.
55 J. Premkumar, *Chem. Mater.*, 2004, **16**, 3980–3981.
56 R. Katoh, M. Kasuya, S. Kodate, A. Furube, N. Fuke and N. Koide, *J. Phys. Chem. C*, 2009, **113**, 20738–20744.
57 D. F. Watson and G. J. Meyer, *Coord. Chem. Rev.*, 2004, **248**, 1391–1406.
58 D. Kuciauskas, J. E. Monat, R. Villahermosa, H. B. Gray, N. S. Lewis and J. K. McCusker, *J. Phys. Chem. B*, 2002, **106**, 9347–9358.
59 C. Mahala, M. D. Sharma and M. Basu, *Inorg. Chem.*, 2020, **59**, 6988–6999.
60 H. Ma, Z. J. Wang, W. Zhao, H. Ren, H. Y. Zhu, Y. H. Chi and W. Y. Guo, *J. Phys. Chem. Lett.*, 2022, **13**, 8484–8494.
61 J. W. Xia, N. Karjule, L. Abisdris, M. Volokh and M. Shalom, *Chem. Mater.*, 2020, **32**, 5845–5853.
62 L. Chen, J. Duan, P. H. Du, W. L. Sun, B. Lai and W. Liu, *Water Res.*, 2022, **221**, 118747.
63 X. W. Wang, Z. Han, L. H. Yu, C. T. Liu, Y. F. Liu and G. Wu, *ACS Sustainable Chem. Eng.*, 2018, **6**, 14542–14553.
64 S. Fukuzumi, Y. M. Lee and W. Nam, *Chem. - Eur. J.*, 2018, **24**, 5016–5031.
65 C. A. Bignozzi, S. Caramori, V. Cristino, R. Argazzi, L. Meda and A. Tacca, *Chem. Soc. Rev.*, 2012, **42**, 2228–2246.
66 J. W. Huang, Y. Zhang and Y. Ding, *ACS Catal.*, 2017, **7**, 1841–1845.
67 H. Y. Wang, E. Mijangos, S. Ott and A. Thapper, *Angew. Chem., Int. Ed.*, 2014, **53**, 14499–14502.